A reductive aminase from *Aspergillus oryzae*

Godwin A. Aleku [a], Scott P. France,[a] Henry Man,[b] Juan Mangas-Sanchez,[a] Sarah L. Montgomery,[a] Mahima Sharma,[b] Friedemann Leipold,[a] Shahed Hussain,[a] Gideon Grogan[b]* and Nicholas J. Turner [a]*.

a. *School of Chemistry, University of Manchester, Manchester Institute of Biotechnology, 131 Princess Street, Manchester M1 7DN, UK.*

b. *York Structural Biology Laboratory, Department of Chemistry, University of York, Heslington, York, YO10 5DD UK.*

Abstract

Reductive amination is one of the most important methods for the synthesis of chiral amines. Here we report the discovery of an NADP(H)-dependent reductive aminase from *Aspergillus oryzae* (*Asp*RedAm, Uniprot code Q2TW47) which can catalyse the reductive coupling of a broad set of carbonyl compounds with a variety of primary and secondary amines with up to >98% conversion and with up to >98% enantiomeric excess. In cases where both carbonyl and amine show high reactivity, it is possible to employ a 1:1 ratio of the substrates, forming amine products with up to 94% conversion. Steady-state kinetic studies establish that the enzyme is capable of catalysing imine formation as well as reduction. Crystal structures of *Asp*RedAm in complex with NADP(H) and also with both NADP(H) and the pharmaceutical ingredient (*R*)-rasagiline are reported. We also demonstrate preparative scale reductive aminations with wild-type and Q240A variant biocatalysts displaying total turnover numbers of up to 32,000 and space time yields up to 3.73 g L^{-1} d^{-1}.

An analysis of drugs approved by the FDA in recent years reveals that *ca*. 40% of new chemical entities (NCEs) contain one or more chiral amine building blocks.[1] This sustained prevalence of chiral amines in

APIs has driven the development of new and efficient catalytic methods for chiral amine synthesis that have broad application.[2–6] In this context, the reductive amination of ketones is one of the most powerful and frequently employed reactions for amine synthesis, enabling a wide range of ketones to be coupled to primary and secondary amines.[7–11]

In view of the fact that the products are often chiral, there is an increasing desire to develop asymmetric variants of this reaction, particularly utilising chemo- or biocatalysis. Specifically, transition metal-catalysed reductive amination and enantioselective enamide reduction approaches[8] to chiral amines have received considerable attention as well as biocatalytic routes employing transaminases,[6,12–14] ammonia lyases[15–17] or monoamine oxidases.[18–20]

In addition, a number of distinct enzyme families have previously been reported to catalyse the reductive amination of ketones. The NADPH-dependent octopine dehydrogenases (OctDHs) catalyse the coupling of α-amino acids with α-keto acids and have been the focus of recent attempts to broaden their substrate range using protein engineering.[21] Amino acid dehydrogenases (AADHs) perform aminations of α-keto acids with ammonia by first catalysing formation of α-imino acids followed by NADPH-dependent reduction to yield α-amino acids. Although AADHs have been engineered to accept simple unfunctionalised ketones, they typically show strict specificity for ammonia as the amine nucleophile.[22,23] The related *N*-methyl-amino acid dehydrogenases (NMAADHs) use methylamine to generate the corresponding *N*-methyl-amino acids.[24] Recently, reductive amination has also been demonstrated using imine reductases (IREDs).[25–28] However, the reactions have involved the use of large quantities of IRED enzyme, and ratios of amine to ketone ranging from *ca*. 50:1[26] to 12.5:1[27] in order to achieve the conversions. This low reactivity of IREDs for the catalysis of reductive amination is almost certainly due to the fact that their principal role is to catalyse the reduction of preformed cyclic imines.[29] For example, we[30–34] and others[25,26,35,36] have shown that IREDs catalyse the asymmetric reduction of a wide range of 5-, 6-, and 7-membered imines with good conversions and high enantioselectivity.

Importantly, from a mechanistic viewpoint, OctDHs, AADHs and NMAADHs have been shown to catalyse imine formation, whereas the IREDs described so far have not.[25–27] Thus, one important goal is to identify an enzyme scaffold which can combine (i) high activity for imine formation from ketone and amine; (ii) high enantioselectivity for imine reduction and (iii) broad substrate tolerance with respect to both amines and ketones. Herein we report our efforts to find and develop an enzyme that possesses these properties through the discovery and investigation of a reductive aminase (RedAm) (Figure 1).

Results and Discussion

Identification of Asp*RedAm*

A reductive aminase from *Aspergillus oryzae* (*Asp*RedAm), the first IRED homolog from a eukaryotic source, was initially identified based upon its sequence similarity to known IREDs including those from *Amycolatopsis orientalis* (*Ao*IRED)[34] and *Streptomyces* sp.[37–39] Those IREDs have been shown to possess high activity for imine reduction but modest to poor activity for reductive amination. Following cloning and expression of the gene encoding *Asp*RedAm in *E. coli*, the purified enzyme was revealed to have remarkable potency as a catalyst of reductive amination. The characterisation of *Asp*RedAm using biotransformations, kinetic and structural studies suggests it is representative of a subclass of IREDs that have evolved to possess a particular capability for reductive amination reactions.

Investigation of substrate specificity of Asp*RedAm*

The relative specific activity of *Asp*RedAm towards a representative library of carbonyl acceptors **1**-**32** was determined using propargylamine **a** and methylamine **g** as substrates, with the amine and NADPH concentrations maintained at saturation (Supplementary Section 7.1, Table 10). In order to assess the amine substrate scope, the relative specific activities of *Asp*RedAm with cyclohexanone **1** and 4-phenyl-2-butanone **17** were also measured towards amines **a**-**s** (Supplementary Section 7.2, Table 11). *Asp*RedAm exhibited higher specific activity for **1** with **a** (6.68 U mg^{-1}) and with allylamine **c** (7.68 U mg^{-1})

compared to **g** (2.23 U mg^{-1}), highlighting the contribution of the amine partner to the catalytic rates. A clear preference for cyclic ketones was observed (e.g. **1** and **4**) and C5 or C6 linear ketones and aldehydes (e.g. hexanal **3**, 2,5-hexanedione **5**, 2-hexanone **6**) were transformed faster than C4 carbonyl compounds (e.g. 2-butanone **26**). The screening of amine nucleophiles revealed a greater activity of *Asp*RedAm towards primary amines, especially unsaturated aliphatic amines (**a** and **c**). Excellent activity was observed with cyclopropylamine **b**, however the activity was significantly lower when isopropylamine **n** was used as a nucleophile. In the presence of reactive carbonyl acceptors (e.g. **1**), amination with various amines, including *N*-methylprop-1-yn-1-amine **j**, pyrrolidine **l**, piperidine **p**, ammonia **k** and hydroxylamine **q**, proceeded with activities of up to 0.7 U mg^{-1}. However, with a less reactive carbonyl acceptor (e.g. **17**), lower rates were observed with these reacting partners, although primary amines were tolerated.

By combining the data of relative specific activities towards the carbonyl acceptors and amine partners (Supplementary Section 7, Table 10 and Table 11) we generated a reactivity chart to act as a predictive tool for the likely outcome of reductive amination between specific ketones and amines (Figure 2). The chart was constructed by combining the average relative activities of representative carbonyl compounds, measured with two amine nucleophiles (**a** and **g**), and plotting this against the average relative specific activities of amine nucleophiles measured with two ketones (**1** and **17**). The carbonyl compounds and amines were arranged in Groups I-IV and Groups A-C respectively based on their average relative specific activity value. For ketone-amine combinations that have high relative specific activities for both reacting partners (*i.e.* Groups I and II *vs*. Group A, Figure 2) it is likely that high-yielding reductive aminations can be achieved with *Asp*RedAm with near stoichiometric equivalents of ketone and amine. Increasing the amine equivalents can improve conversions for substrates that have less favourable specific activities (*i.e.* Groups III and IV *vs*. Group B and C, Figure 2).

Using the reactivity chart as a guide, a series of biotransformations was performed with a range of carbonyl and amine combinations (Table 1). *Asp*RedAm reactions with both cyclic and acyclic ketones afforded products in moderate to excellent conversion and enantioselectivity. In several cases, equimolar concentrations of ketone and amine gave high conversions (Table 1, products **1a**, **1b**, **1c**, **1m**), which is indicative of genuine *Asp*RedAm-catalysed reductive amination processes. Ammonia **k** and secondary amines **l** and **p** were also accepted as reacting partners when coupled with particularly active carbonyls (Table 1, products **1k**, **9k**, **19p**, **19p**). In the *Asp*RedAm-catalysed reaction between benzaldehyde **19** and **k**, the initial product of reductive amination was benzylamine **m** which acts as an amine reacting partner for a second reductive amination with the ketone substrate, resulting in product **19m**. Reductive amination of ethyl levulinate **10** afforded *N*-alkylpyrrolidinones (**10a**-**b**) as products following spontaneous cyclisation. Interestingly, *Asp*RedAm could also distinguish to some extent between (*R*)- and (*S*)-*sec*-butylamine **t** as the amine coupling partner with (*S*)-**t** giving higher conversion. Furthermore, *Asp*RedAm was able to directly produce the active pharmaceutical ingredient (API) (*R*)-rasagiline **29a** starting from 1-indanone **29** and **a** in 64% conversion and 95% *e.e*.

Asp*RedAm versus IREDs*

As an IRED homolog, purified *Asp*RedAm displayed broad substrate scope in the reduction of cyclic and preformed imines and iminium ions, allowing access to secondary and tertiary amines. For example, dihydroisoquinoline derivative **45** was transformed to the natural product salsolidine **46** with >99% conversion and >99% *e*.*e*. (Supplementary Section 8). *Asp*RedAm was also able to act in the reverse, oxidative direction and exhibited activity in the dehydrogenation of amines to yield imines. The highest activity was found for 1-methyl-tetrahydroquinoline **34** and acyclic amines were also found to be transformed (Supplementary Section 7, Table 12). This reactivity was exploited in the efficient kinetic resolution of rasagiline *rac*-**29a** to give the (*S*)-enantiomer in 49% conversion and 99% *e*.*e*. Interestingly, the enzyme displayed regioselectivity in the deamination as only indanone **29**, **a** and (*S*)-**29a** were detected after a 24-hour biotransformation of *rac*-**29a**.

To further investigate the unusual catalytic features of *Asp*RedAm, we compared its reductive amination activity to those of the IRED from *Streptomyces* sp. GF3587 (*R*-IRED)[31,38] and the *Amycolatopsis orientalis* IRED (*Ao*IRED).[34] For enzymes only capable of reducing preformed imines, we anticipated that reductive amination activity with aldehydes would be highly dependent on pH, as it has been reported that spontaneous imine formation between benzaldehyde and methylamine in aqueous solution is insignificant at pH 7.6 (4%) but considerable at pH 9.0 (87%).[26] Conversely, for ketones, spontaneous imine formation is negligible at both pHs and, therefore, reductive amination activity is less likely to be pH dependent.

Initial rate measurements of the selected IREDs were performed at pH 7.0 and 9.0 using **1** and **3** with **c** (Supplementary Section 12). *Asp*RedAm displayed much higher specific activities than *R*-IRED and *Ao*IRED for the reductive amination of both **1** and **3** regardless of pH. In the reductive amination of **3**, an approximate 20-fold improvement in specific activity was observed for *R*-IRED and *Ao*IRED when the pH

was increased from 7.0 to 9.0. This correlates with the difference in the imine concentration in aqueous media at different pHs that was previously reported and further suggests that these IREDs rely on preformed imine in solution which they are then able to reduce.[26] Remarkably, the specific activity of *Asp*RedAm only increased 1.3-fold, showing that the spontaneous imine formation in solution is not essential for this enzyme. For the reductive amination of **1**, there was no significant change in activity from pH 7.0 to 9.0 with *Asp*RedAm, *Ao*IRED or *R*-IRED. The high specific activity of *Asp*RedAm at pH 7.0 and pH 9.0 for reactions with both **1** and **3** is indicative of the role of *Asp*RedAm in catalysing both the formation of imine and its subsequent reduction. The differences between *Asp*RedAm and other IREDs are further highlighted by sequence comparison and structure studies, reported herein.

A Kinetic Model for Asp*RedAm Activity*

*Asp*RedAm-catalysed reductive amination of ketones follows the Michaelis–Menten model based on initial rate studies. For a selected substrate panel, *Asp*RedAm exhibited high activity in many cases; for example, the k_{cat} for *Asp*RedAm-catalysed reductive amination of **1** and **c** was 5 s^{-1} (Supplementary Section 6.2). In order to further probe the mechanism of *Asp*RedAm-catalysed reductive amination we carried out detailed steady-state kinetic studies using **1** and **g** as substrates (Supplementary Section 6). We simultaneously varied the concentration of **1** and **g** while NADPH was held at saturation; the resulting double-reciprocal plots ($1/v_i$ *versus* 1/[**1**]) yielded patterns of lines that intersected to the left of the 1/v axis. When **g** was held at saturation and the NADPH concentration varied at different fixed concentrations of **1**, a similar intersecting pattern of lines was obtained. The intersecting lines were also obtained when **1** was held at a constant level, and NADPH was varied at fixed concentration of **g**. These patterns are consistent with a sequential mechanism and rule out a ping-pong mechanism for *Asp*RedAm activity.

To investigate the order of substrate addition and product release, product inhibition studies were conducted in the forward and reverse directions (Supplementary Section 6.4). In the forward direction, inhibition by $NADP^+$ is linearly competitive with respect to NADPH, uncompetitive with respect to **1** and non-competitive with respect to **g**. In the reverse reaction, NADPH behaves as a linear competitive and non-competitive inhibitor with respect to $NADP^+$ and **1g** respectively. This inhibition pattern indicates that NADPH is the first substrate to bind while $NADP^+$ is the last product released in the forward reaction.[40,41] Inhibition by **1g** was non-competitive with respect to NADPH, **1** and **g**. This pattern is consistent with **1g** being the first product to be released in the forward direction.[40,41] In the reverse direction, **g** behaves as a non-competitive inhibitor with respect to $NADP^+$ and **1g** indicating that **g** is the first substrate to be released in the oxidation of **1g** and the last substrate to bind in the forward direction. Inhibition by **1** was uncompetitive with respect to $NADP^+$ and **1g** in the forward direction, as would be expected of the substrate binding second in the sequence.

The kinetic behaviour observed when the concentrations of two substrates were simultaneously varied alongside the patterns of inhibition obtained from the product inhibition studies showed that *Asp*RedAm-catalysed reductive coupling of **1** and **g** to form **1g** follows an ordered sequential Ter Bi mechanism. The cofactor NADPH, the ketone **1** and the amine **g** are added to the enzyme in that sequence followed by the release of product **1g** and $NADP^+$ (Figure 3). The *Asp*RedAm-catalysed reductive amination follows the kinetic model displayed by *N*-methyl-L-amino acid dehydrogenase from *Pseudomonas putida* with the same order of binding of substrates.[24] Other enzymes that catalyse imine formation also operate via a Ter Bi mechanism such as number of α-keto dehydrogenases[42–46] and opine dehydrogenases (OpDHs)[41,47], however, the order of ketone and amine binding can be different.

Crystal Structure of AspRedAm and mutagenesis studies

The exceptional properties of *Asp*RedAm prompted us to examine its structure using X-ray crystallography, and to compare it with IREDs that are not capable of catalysing equimolar reductive amination reactions. Co-crystallisation of *Asp*RedAm with **29**, amine **a** and NADPH resulted in a ternary complex, in which both NADP(H) and the product, (*R*)-**29a**, were found in the active site. The crystals were in the *P*1 space group, and four dimers were found in the asymmetric unit. *Asp*RedAm possesses the canonical IRED fold, in which two monomers, each made up of an *N*-terminal Rossman domain and a *C*-terminal helical bundle connected by a long inter-domain α-helix, associate to form a functional dimer in which the active site forms at the interface between the *N*- and *C*-terminal domains of different monomers (Figure 4A). In contrast to other IRED structures however, the ternary complex of *Asp*RedAm is significantly more compact, with a relative movement between domains closing the active site over the NADP(H) and the product ligand to form a much smaller active site than has been observed in 'open' forms of IREDs previously.[31–34,48,49]

The ligand was bound within a hydrophobic pocket previously identified in the IRED from *Ao*IRED[34] adjacent to the (*Si*)-face of the nicotinamide ring of NAD(P)H. The ligand is somewhat mobile in the eight active sites in the asymmetric unit, but the nitrogen atom of the amine is 3.2-4.9 Å (4.5 Å in the case shown in Figure 4B) from the phenolic hydroxyl of Y177, suggesting a role in either proton donation or product anchoring by this residue. Mutation of Y177 to alanine resulted in a mutant Y177A with about a 30-fold decrease in reductive aminase activity compared to the wild-type enzyme (Figure 4C). The ligand conformation in Figure 4B also positions the electrophilic carbon of the amine product at between approximately 3.4 and 4.2 Å from C4 of the nicotinamide ring of NAD(P)H (3.8 Å in the case shown in Figure 4B), an ideal distance for hydride delivery/acceptance. It was also interesting that mutation of D169, which has been thought to have a role in catalysis in some IREDs,[33] resulted in variants D169A and

D169N of significantly reduced reductive aminase activity (Figure 4C). Both mutants showed a *ca*. 200-fold decrease in reductive amination activity compared to the wild-type enzyme. Other residues of possible significance are N93, which hydrogen bonds to D169, Q240 and M239 at the front of the picture in Figure 4B that are brought nearly into contact with the ligand upon closure of the active site, and W210 at the back of the picture, which helps to complete the hydrophobic pocket.

The characterisation of the active site of *Asp*RedAm provided a basis for searching the sequence databases for other enzymes of similar properties, and also to compare the enzyme against IREDs reported previously, which have not displayed equimolar reductive aminase activity. A number of other sequences from filamentous fungi, including *Aspergillus terreus* (*At*RedAm) and *Ajellomyces dermatitidis* (*Ad*RedAm) were identified that each contained residues equivalent to N93, D169, Y177, W210, M239 and Q240 in *Asp*RedAm. The genes encoding *At*RedAm and *Ad*RedAm were cloned and expressed in *E. coli* and, following purification of the enzymes, we were able to confirm asymmetric reductive amination using a 1:1 ratio of amines **a**, **c** and **g** and ketone **1** as a property of these enzymes (Supplementary Section 11.3, Table 17). A phylogenetic tree that compares these fungal RedAms with sequences of enzymes for which non-equimolar reductive amination reactions have been reported[26,27,48] shows that fungal RedAms form a distinct sub-group (Supplementary Section 11.1, Figure 67). Analysis of the sequences of these enzymes reveals that while one or two bacterial IREDs may feature some of the active site residues of RedAms, none of the bacterial homologs is likely to contain all of them within the active site (Supplementary Section 11.2, Table 16). IR_9 and IR_23, described by Wetzl and co-workers[27,35] are most similar, containing five and four out of the six residues respectively, but each has a threonine residue in the place of asparagine in positions equivalent to 93 in RedAms. A direct comparison of *Asp*RedAm with IR_23 shows that the former catalysed the formation of amine **1g** with 84% conversion at a ketone:amine ratio of 1:2; IR_23 was reported to catalyse this transformation with 80% conversion, but only at a ketone:amine ratio of 1:12.5.[27] Whilst we cannot conclude that these six

residues uniquely describe the requirements of a RedAm active site, their identification should prove a useful guide to the identification of further RedAm enzymes in the sequence databases.

The structure of *Asp*RedAm suggested that W210 and Q240 may be good target residues to mutate in order to alter substrate specificity. Indeed, the W210A variant displayed a dramatic selectivity switch to yield the antipodal (*S*)-amine products upon the reductive amination of **17** with a variety of amine nucleophiles (Table 2, entries 1-4, Supplementary Section 9.1, Figure 66). (*S*)-Selectivity was also observed when **a** was reductively coupled with 2-tetralone **9** (Table 2, entry 6), as well as in the coupling of **10** with **c** to form the *N*-substituted lactam **10c**. Variant W210S displayed similar stereoselective properties to W210A, with the (*S*)-amine products formed upon the reductive amination of a panel of substrates (Table 2). From the determination of the kinetic parameters, both W210A and W210S displayed similar activity profiles although W210A appeared to be slightly more active (Supplementary Section 9, Table 14). Interestingly, the Q240A variant displayed significant improvements in (*R*)-selectivity for most substrates compared to the wild-type enzyme. For example, the enantioselectivity in the reductive amination of **17** with **c** was greatly improved (94% *e.e.*) compared to the wild-type (30% *e.e*. Table 2, entry 1). The Q240A variant was also capable of coupling **k** to **17** to yield the primary chiral amine **17k** in excellent *e.e.* (>98%). The significant improvement in the (*R*)-selectivity of *Asp*RedAm Q240A also permitted the successful synthesis of (*R*)-**29a** in >98% conversion with >98% *e.e.* using this mutant.

Preparative-Scale Reductive Aminations using AspRedAm

To test the synthetic applicability of *Asp*RedAm, a series of preparative-scale reactions were performed. Taking **1** and **g** as model substrates, certain process parameters were investigated on an analytical-scale prior to implementing the reaction on a larger scale. The concentration of ketone, the number of amine equivalents and the enzyme loading were investigated (Supplementary Section 13, Table 18).

Interestingly, excellent conversion (>97%) could be achieved using 50 mM **1**, 2 amine equivalents and 0.1 mg mL^{-1} *Asp*RedAm and so these conditions were employed for the 100 mg scale synthesis of **1g**, which was isolated as a hydrochloride salt, in 75% yield. A variety of other reductive amination products **1a**, **6g**, **10a** and **17g** were successfully recovered with either wild-type *Asp*RedAm or the Q240A variant on a preparative scale to afford products in good to excellent isolated yields of 70%, 70%, 48% and 78% respectively after hydrochloride salt formation or column chromatography (Supplementary Section 13). These reactions compare favourably with other preparative biocatalytic processes[50,51] with total turnover numbers (TTNs) up to 32,000, turnover frequencies (TOFs) up to 300 min^{-1} and space time yields (STYs) up to 3.73 g L^{-1} d^{-1}.

Conclusion

In summary, we report the discovery and characterization of a reductive aminase from *Aspergillus oryzae* (*Asp*RedAm) which has been shown to possess remarkably high activity for the reductive amination of ketones and amines, often with high stereoselectivity and in some cases with ketone:amine ratios as low as 1:1. By examining the relative activities of a broad range of different amines and ketones it has been possible to construct a predictive reactivity chart in which the likely outcome of a reductive amination reaction can be appraised. We also present detailed kinetic studies, to support the order of substrate binding and product release, together with an X-ray crystal structure of a ternary complex of *Asp*RedAm which has been used to inform mutagenesis studies and has allowed us to identify key active-site residues that may be involved in ligand binding and catalysis. The demonstrated activity in the reductive amination of aldehydes between pH 7.0 and 9.0 provides further evidence that *Asp*RedAm catalyses imine formation. Finally we have illustrated the synthetic potential of *Asp*RedAm through the reductive amination of a number of ketone substrates and successfully demonstrated the preparative-scale synthesis of a selection of amine products. Taken together, these

results serve to highlight RedAms as an important sub-group of IREDs that possess unique and attractive properties for the biocatalytic preparation of industrially important amines.

EXPERIMENTAL SECTION

General

For full details of synthetic procedures and characterisation data, see Supplementary Information.

Gene synthesis, cloning, expression and protein purification

The codon-optimized gene sequence encoding *Asp*RedAm (GenBank accession number, KY327363) was sub-cloned into pET28a-(+) vector form pET 28a-His-*Asp*RedAm plasmid (Figure S2). Site-directed mutagenesis for the creation of *Asp*RedAm variants were performed using primers as listed in the Supplementary Information (Section 3.2). Cultivation was performed in 500 mL 2x YT broth medium with kanamycin (30 μg mL^{-1}). Cultures were initially incubated at 37°C with shaking at 250 rpm. At an optical density (OD_{600nm}) of between 0.6 and 0.8, isopropyl β-D-1-thiogalactopyranoside (IPTG) was added to a final concentration of 0.5 mM to induce the expression of *Asp*RedAm. Incubation was continued at 20°C and 250 rpm for 18 h. Cells were then harvested by centrifugation and resuspended in sodium phosphate buffer (100 mM, pH 7.5). Cells were disrupted by ultrasonication at 0°C. The enzyme was purified from the clarified lysate by Ni-affinity chromatography. To further purify the protein for crystallisation, size exclusion chromatography (SEC) was performed in Tris-HCl buffer (50 mM, pH 8.0) containing 500 mM NaCl. The protein concentration was determined using the Bradford assay against BSA as a concentration standard. Further details and general information on strains and plasmids, and details of gene design and cloning protocols can be found in the Supplementary Information (Section 3).

Biotransformations

Typical procedure for *Asp*RedAm-catalysed reductive amination: a 500 µL reaction mixture contained 30 mM D-glucose, 0.4 mg mL^{-1} GDH (Codexis, CDX-901), 1 mM $NADP^+$, 1 mg mL^{-1} purified *Asp*RedAm, 5 mM carbonyl compound, the appropriate ratio of amine nucleophile (in buffer adjusted to pH 9.0) and 2% (v/v) dimethylformamide or dimethylsulfoxide. The reaction volume was made up to 500 µL with Tris-HCl buffer (100 mM, pH 9.0). Reactions were incubated at 25°C with shaking at 250 rpm for 24 h, after which they were quenched by the addition of 30 µL of 10 M NaOH and extracted twice with 500 µL *tert*-butyl methyl ether. The organic fractions were combined and dried over anhydrous $MgSO_4$ and analysed by HPLC or GC-FID on a chiral stationary phase. For further details see the Supplementary Information (Section 4 & 5).

Preparative-scale reactions were run using 100 mM D-glucose, 0.5 mM $NADP^+$, 0.3 mg mL^{-1} GDH, 50 mM or 10 mM ketone, 2, 5 or 20 equivalents of amine, 0.1 to 0.5 mg mL^{-1} purified wild-type *Asp*RedAm or 1.0 mg mL^{-1} *Asp*RedAm Q240A variant in 100 mM pH 9.0 Tris buffer. Reactions were incubated at 20°C or 30°C, 250 rpm for 24 h. The reaction was basified to pH 12 with 10 M NaOH solution and the product extracted into diethyl ether or dichloromethane with intermediate centrifugation (4°C, 2,831 rcf, 5 min) to improve the separation of phases. The organic layers were combined, dried over anhydrous $MgSO_4$ and the solvent carefully concentrated. The residue was dissolved in dry diethyl ether and acidified with a solution of 2 M HCl in diethyl ether or purified by column chromatography. Further details can be found in the Supplementary Information (Section 13).

Kinetic Assays

The reductive aminase activity was measured using a modified method to that previously reported.[24,52] For substrate specificity screening, a typical reaction mixture contained 15 mM carbonyl compound, 60 mM amine nucleophile from buffer stock adjusted to pH 9.3, 0.3 mM NADPH, 1 % (v/v) dimethylsulfoxide and 5-100 µg of purified *Asp*RedAm in a total volume of 200 µL (100 mM sodium

tetraborate, pH 9). Activity measurements were performed in triplicate at 340 nm (ε = 6.22 mM^{-1} cm^{-1}) or 370 nm (ε = 2.216 mM^{-1} cm^{-1}) using a Tecan infinite M200 microplate reader (Tecan Group, Switzerland).

Steady state kinetic measurements were performed with various concentrations of one substrate at different fixed concentrations of the second substrate while the third substrate was held at a constant level. Double reciprocal plots were obtained and line patterns were examined against rate equations describing sequential mechanisms. Product inhibition studies for the reductive amination of **1** and **g**, and the deamination of **1g** were performed with various concentrations of the one substrate and fixed saturating concentrations of the other substrates in the presence of the product (inhibitor). Double reciprocal plots obtained were examined and data were fitted into equation describing competitive, non-competitive and uncompetitive inhibition. The reaction was initiated by the addition of purified *Asp*RedAm to the mixture. A unit of *Asp*RedAm was equal to the amount of the pure enzyme required to consume 1 µmol NADPH/ $NADP^+$ per min. Activity measurements were performed in triplicate and kinetic constants were determined through nonlinear regression based on Michaelis–Menten kinetics (QtiPlot software). For further details see Supplementary Information (Section 6).

Protein Crystallization

Purified *Asp*RedAm was subjected to crystallisation trials using a range of commercially-available screens in 96-well sitting-drop format in which each drop consisted of 150 nL protein and 150 nL of precipitant reservoir solution. Crystallization experiments gave two structures of *Asp*RedAm: an NADP(H) complex and also a ternary complex with NADP(H) and (*R*)-**29a**. For further details see Supplementary Information (Section 10). Crystals that diffracted to a resolution of equal to, or better than, 3 Å resolution were retained for dataset collection at the Diamond Light Source synchrotron. The coordinate files and structure factors have been deposited in the Protein DataBank (PDB) with coordinate accession numbers 5g6r [*Asp*RedAm-NADP(H)] and 5g6s [*Asp*RedAm-NADP(H)-(*R*)-rasagiline complex].

Data availability

The authors declare that the data supporting the findings of this study are available within the paper and its supplementary information files. Additionally, sequence data has been deposited in Genbank with the accession code KY327363 (https://www.ncbi.nlm.nih.gov/nuccore/KY327363) and the coordinate files and structure factors have been deposited in the Protein DataBank (PDB) with coordinate accession numbers 5g6r [*Asp*RedAm-NADP(H)] and 5g6s [*Asp*RedAm-NADP(H)-(*R*)-rasagiline complex].

Author Contributions

N.J.T. and G.G. initiated the study and directed the project. G.A.A., M.S. and F.L. cloned and expressed the enzymes. G.A.A. performed the kinetics and mutagenesis studies. G.A.A., S.P.F., J.M.S., S.L.M. and M.S. performed biotransformations. H.M. obtained crystal structures. S.P.F., J.M.S., S.L.M., G.A.A. and S.H. chemically synthesised substrates and product standards.

Acknowledgements

We thank the industrial affiliates of the Centre of Excellence for Biocatalysis, Biotransformations and Biomanufacture (CoEBio3) for awarding studentships to G.A.A. and H.M.. S.P.F. was supported by a CASE studentship from Pfizer. J.M.S and M.S. were funded by grant BB/M006832/1 from the UK Biotechnology and Biological Sciences Research Council. S.L.M. was supported by a CASE studentship from Johnson Matthey. S.H. was supported by a CASE studentship from AstraZeneca. F.L. received support from the Innovative Medicines Initiative Joint Undertaking under the grant agreement no. 115360 (Chemical manufacturing methods for the 21st century pharmaceutical industries, CHEM21) and the European Union's Seventh Framework Program (FP7/2007-2013) and EFPIA companies' in-kind contributions. We thank Dr Johan P. Turkenburg and Mr Sam Hart for assistance with X-ray data collection, and the Diamond Light Source for access to beamlines I02 and I03 under proposal number

mx-9948. The authors would also like to thank Mr Joan Citoler for assistance with mutagenesis. N.J.T. also acknowledges the Royal Society for a Wolfson Research Merit Award.

References:

1. Jarvis, L. M. The Year in New Drugs. *Chem. Eng. News* 12–17 (2016).
2. Topczewski, J. J., Cabrera, P. J., Saper, N. I. & Sanford, M. S. Palladium-catalysed transannular C–H functionalization of alicyclic amines. *Nature* **531,** 220–224 (2016).
3. Mutti, F. G., Knaus, T., Scrutton, N. S., Breuer, M. & Turner, N. J. Conversion of alcohols to enantiopure amines through dual-enzyme hydrogen-borrowing cascades. *Science.* **349,** 1525–1529 (2015).
4. Wanner, B., Kreituss, I., Gutierrez, O., Kozlowski, M. C. & Bode, J. W. Catalytic kinetic resolution of disubstituted piperidines by enantioselective acylation: Synthetic utility and mechanistic insights. *J. Am. Chem. Soc.* **137,** 11491–11497 (2015).
5. Xu, H., Chowdhury, S. & Ellman, J. A. Asymmetric synthesis of amines using *tert*-butanesulfinamide. *Nat. Protoc.* **8,** 2271–2280 (2013).
6. Savile, C. K. *et al.* Biocatalytic asymmetric synthesis of chiral amines from ketones applied to sitagliptin manufacture. *Science.* **329,** 305–309 (2010).
7. Huang, H., Liu, X., Zhou, L., Chang, M. & Zhang, X. Direct asymmetric reductive amination for the synthesis of chiral β-arylamines. *Angew. Chem,. Int. Ed.* **55,** 5309–5312 (2016).
8. Nugent, T. C. & El-Shazly, M. Chiral amine synthesis - Recent developments and trends for enamide reduction, reductive amination, and imine reduction. *Adv. Synth. Catal.* **352,** 753–819 (2010).
9. Li, C., Villa-Marcos, B. & Xiao, J. Metal-bronsted acid cooperative catalysis for asymmetric reductive amination. *J. Am. Chem. Soc.* **131,** 6967–6969 (2009).
10. Schrittwieser, J. H., Velikogne, S. & Kroutil, W. Biocatalytic imine reduction and reductive amination of ketones. *Adv. Synth. Catal.* **357,** 1655–1685 (2015).
11. Seiple, I. B. *et al.* A platform for the discovery of new macrolide antibiotics. *Nature* **533,** 338–345

(2016).

12. Mathew, S. & Yun, H. ω-Transaminases for the production of optically pure amines and unnatural amino acids. *ACS Catal.* **2,** 993–1001 (2012).

13. Simon, R. C., Richter, N., Busto, E. & Kroutil, W. Recent developments of cascade reactions involving ω-transaminases. *ACS Catal.* **4,** 129–143 (2014).

14. Pavlidis, I. V. *et al.* Identification of (*S*)-selective transaminases for the asymmetric synthesis of bulky chiral amines. *Nat. Chem.* **8,** 1076–7082 (2016).

15. Weise, N. J., Parmeggiani, F., Ahmed, S. T. & Turner, N. J. The bacterial ammonia lyase EncP: A tunable biocatalyst for the synthesis of unnatural amino acids. *J. Am. Chem. Soc.* **137,** 12977–12983 (2015).

16. DeLange, B. *et al.* Asymmetric synthesis of (*S*)-2-indolinecarboxylic acid by combining biocatalysis and homogeneous catalysis. *ChemCatChem* **3,** 289–292 (2011).

17. Parmeggiani, F., Lovelock, S. L., Weise, N. J., Ahmed, S. T. & Turner, N. J. Synthesis of D- and L-phenylalanine derivatives by phenylalanine ammonia lyases: A multienzymatic cascade process. *Angew. Chem., Int. Ed.* **54,** 4608–4611 (2015).

18. Ghislieri, D. *et al.* Engineering an enantioselective amine oxidase for the synthesis of pharmaceutical building blocks and alkaloid natural products. *J. Am. Chem. Soc.* **135,** 10863–10869 (2013).

19. Heath, R. S., Pontini, M., Bechi, B. & Turner, N. J. Development of an *R*-selective amine oxidase with broad substrate specificity and high enantioselectivity. *ChemCatChem* **6,** 996–1002 (2014).

20. Yasukawa, K., Nakano, S. & Asano, Y. Tailoring D-amino acid oxidase from the pig kidney to *R*-stereoselective amine oxidase and its use in the deracemization of α -methylbenzylamine. *Angew. Chem. Int. Ed.* **53,** 4428–4431 (2014).

21. Chen, H. *et al.* Engineered imine reductases and methods for the reductive amination of ketone

and amine compounds. US Patent Application 20130302859 (2013).

22. Abrahamson, M. J., Vázquez-Figueroa, E., Woodall, N. B., Moore, J. C. & Bommarius, A. S. Development of an amine dehydrogenase for synthesis of chiral amines. *Angew. Chem., Int. Ed.* **51,** 3969–3972 (2012).

23. Ye, L. J. *et al.* Engineering of amine dehydrogenase for asymmetric reductive amination of ketone by evolving *Rhodococcus* phenylalanine dehydrogenase. *ACS Catal.* **5,** 1119–1122 (2015).

24. Mihara, H. *et al. N*-methyl-L-amino acid dehydrogenase from *Pseudomonas putida*: A novel member of an unusual NAD(P)-dependent oxidoreductase superfamily. *FEBS J.* **272,** 1117–1123 (2005).

25. Huber, T. *et al.* Direct reductive amination of ketones: Structure and activity of *S*-selective imine reductases from *Streptomyces*. *ChemCatChem* **6,** 2248–2252 (2014).

26. Scheller, P. N., Lenz, M., Hammer, S. C., Hauer, B. & Nestl, B. M. Imine reductase-catalyzed intermolecular reductive amination of aldehydes and ketones. *ChemCatChem* **7,** 3239–3242 (2015).

27. Wetzl, D. *et al.* Asymmetric reductive amination of ketones catalyzed by imine reductases. *ChemCatChem* **8,** 2023–2026 (2016).

28. Mangas-Sanchez, J. *et al.* Imine reductases (IREDs). *Curr. Opin. Chem. Biol.* **37,** 19–25 (2017).

29. Leipold, F., Hussain, S., France, S. P. & Turner, N. J. in *Science of Synthesis: Biocatalysis in Organic Synthesis 2* (eds. Faber, K., Fessner, W.-D. & Turner, N. J.) 359–382 (Georg Thieme Verlag, Stuttgart, 2015).

30. Leipold, F., Hussain, S., Ghislieri, D. & Turner, N. J. Asymmetric reduction of cyclic imines catalyzed by a whole-cell biocatalyst containing an (*S*)-imine reductase. *ChemCatChem* **5,** 3505–3508 (2013).

31. Hussain, S. *et al.* An (*R*)-imine reductase biocatalyst for the asymmetric reduction of cyclic imines.

ChemCatChem **7,** 579–583 (2015).

32. Man, H. *et al.* Structure, activity and stereoselectivity of NADPH-dependent oxidoreductases catalysing the *S*-selective reduction of the imine substrate 2-methylpyrroline. *ChemBioChem* **16,** 1052–1059 (2015).

33. Rodriguez-Mata, M. *et al.* Structure and activity of NADPH-dependent reductase Q1EQE0 from *Streptomyces kanamyceticus*, which catalyses the *R*-selective reduction of an imine substrate. *ChemBioChem* **14,** 1372–1379 (2013).

34. Aleku, G. A. *et al.* Stereoselectivity and structural characterization of an imine reductase (IRED) from *Amycolatopsis orientalis*. *ACS Catal.* **6,** 3880–3889 (2016).

35. Wetzl, D. *et al.* Expanding the imine reductase toolbox by exploring the bacterial protein-sequence space. *ChemBioChem* **16,** 1749–1756 (2015).

36. Scheller, P. N. *et al.* Enzyme toolbox: Novel enantio-complimentary imine reductases. *ChemBioChem* **15,** 2201–2204 (2014).

37. Mitsukura, K., Suzuki, M., Tada, K., Yoshida, T. & Nagasawa, T. Asymmetric synthesis of chiral cyclic amine from cyclic imine by bacterial whole-cell catalyst of enantioselective imine reductase. *Org. Biomol. Chem.* **8,** 4533–4535 (2010).

38. Mitsukura, K. *et al.* Purification and characterization of a novel (*R*)-imine reductase from *Streptomyces* sp. GF3587. *Biosci. Biotechnol. Biochem.* **75,** 1778–1782 (2011).

39. Mitsukura, K. *et al.* A NADPH-dependent (*S*)-imine reductase (SIR) from *Streptomyces* sp. GF3546 for asymmetric synthesis of optically active amines: Purification, characterization, gene cloning, and expression. *Appl. Microbiol. Biotechnol.* **97,** 8079–8086 (2013).

40. Whitehead, E. P. Initial rate enzyme kinetics. *Scientia* **113,** 80 (1978).

41. Fujioka, M. & Nakatani, Y. A kinetic study of saccharopine dehydrogenase reaction. *Eur. J. Biochem.* **16,** 180–186 (1970).

42. Heyde, E. & Ainsworth, S. Kinetic studies on the mechanism of the malate dehydrogenase reaction. *J. Biol. Chem.* **243,** 2413–2423 (1968).

43. Ohshima, T., Misono, H. & Soda, K. Properties of crystalline leucine dehydrogenase from *Bacillus sphaericus*. *J. Biol. Chem.* **253,** 5719–5725 (1978).

44. Rife, J. E. & Cleland, W. W. Kinetic mechanism of glutamate dehydrogenase. *Biochemistry* **19,** 2321–2328 (1980).

45. Hochreiter, M. C., Patek, D. R. & Schellenberg, K. A. Catalysis of α-iminoglutarate formation from α-ketoglutarate and ammonia by bovine glutamate dehydrogenase. *J. Biol. Chem.* **247,** 6271–6276 (1972).

46. Stillman, T. J., Baker, P. J., Britton, K. L. & Rice, D. W. Conformational flexibility in glutamate dehydrogenase. Role of water in substrate recognition and catalysis. *Journal of molecular biology* **234,** 1131–1139 (1993).

47. Dairi, T. & Asano, Y. Cloning, nucleotide sequencing, and expression of an opine dehydrogenase gene from *Arthrobacter* sp. strain 1C. *Appl Env. Microbiol* **61,** 3169–3171 (1995).

48. Huber, T. *et al.* Direct reductive amination of ketones: structure and activity of (*S*)-selective imine reductases from *Streptomyces*. *ChemCatChem* **6,** 2248–2252 (2014).

49. Gand, M., Müller, H., Wardenga, R. & Höhne, M. Characterization of three novel enzymes with imine reductase activity. *J. Mol. Catal. B Enzym.* **110,** 126–132 (2014).

50. Rogers, T. A. & Bommarius, A. S. Utilizing simple biochemical measurements to predict lifetime output of biocatalysts in continuous isothermal processes. *Chem. Eng. Sci.* **65,** 2118–2124 (2010).

51. Kohls, H., Steffen-Munsberg, F. & Höhne, M. Recent achievements in developing the biocatalytic toolbox for chiral amine synthesis. *Curr. Opin. Chem. Biol.* **19,** 180–192 (2014).

52. Volner, A., Zoidakis, J. & Abu-Omar, M. M. Order of substrate binding in bacterial phenylalanine hydroxylase and its mechanistic implication for pterin-dependent oxygenases. *J. Biol. Inorg.*

Chem. **8,** 121–128 (2003).

Figure Captions:

Figure 1. Examples of biocatalytic routes to chiral amines *via* monoamine oxidase catalysed resolution, or asymmetric synthesis catalysed by ammonia lyases, transaminases, amine dehydrogenases and imine reductases (IREDs). This work describes the reductive aminase from *Aspergillus oryzae* (*Asp*RedAm) that is capable of performing imine formation as well as reduction to afford a wide variety of chiral amines.

Figure 2. Reactivity chart for *Asp*RedAm-catalysed reactions based on specific activities of a panel of carbonyl compounds and amine reacting partners. a) Chart displaying relative activity of amine/carbonyl pairs in reductive amination reactions. Compounds presented in the plot area are representative examples of products obtained in biotransformations. Conversions of >50% were achieved in all cases when the recommended amine:ketone ratios were used. Framed structures correspond to scaled-up biotransformations with isolated products. b) Carbonyl acceptors and amine nucleophiles arranged in Groups based on their average relative specific activity value. c) Legend for the reactivity chart with specific activity ranking and recommended ratio of amine to carbonyl compound for reductive amination.

Figure 3. Reductive amination of 1 with g and kinetic model for AspRedAm showing sequential cofactor and substrate binding followed by product and cofactor release based on steady-state kinetic studies. Following binding of the nicotinamide cofactor (*i*), ketone is bound (*ii*), followed by the amine (*iii*), followed by enzyme-catalysed imine formation and NADPH-mediated reduction. The amine product is then released (*iv*) prior to $NADP^+$ (*v*).

Figure 4. Structural and mutagenesis data of *Asp*RedAm highlighting essential catalytic residues. a) Dimeric structure of *Asp*RedAm in complex with NADP(H) and (*R*)-29a dimer in which the active site is at the interface between the Rossman fold of one monomer and the C-terminal bundle of its neighbour; b) Active site of *Asp*RedAm at dimer interface. Electron density represents the $2F_o$-F_c (blue) and F_o-F_c (omit, green) maps, the latter obtained prior to refinement of the ligand, and contoured at levels of 1.0 and 2.5σ respectively. Distances

are shown in Ångstroms. c) Kinetic data of *Asp*RedAm wild-type and mutants D169A, D169N and Y177A. Mutation at D169 and Y177 resulted in a marked decrease in activity suggesting essential roles for these residues in catalysis.

Table 1. ***Asp*RedAm-catalysed reductive amination of carbonyl compounds.**

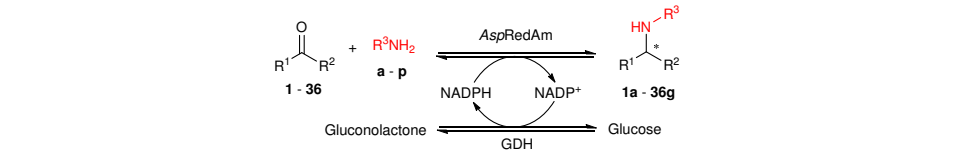

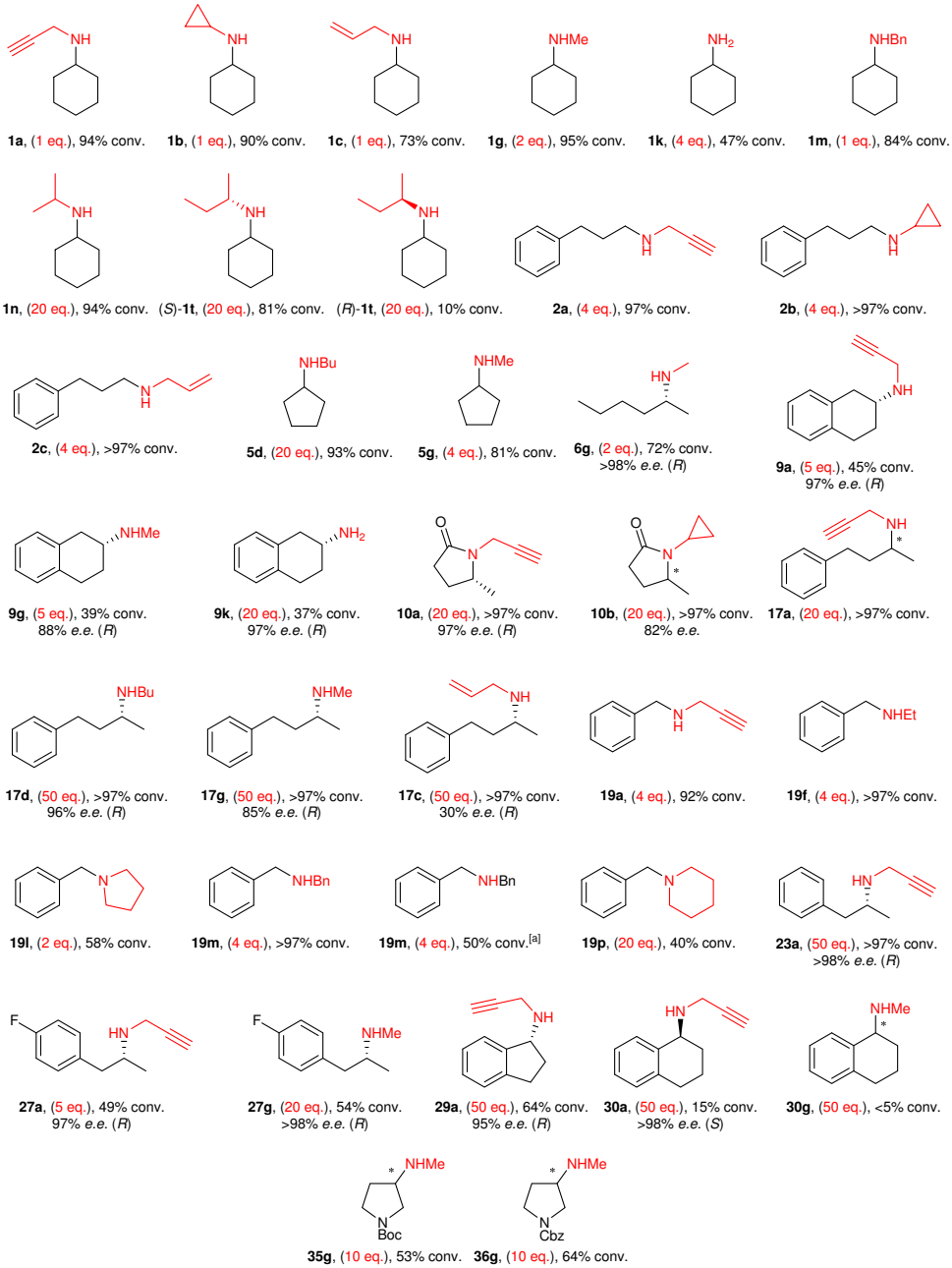

Conversions determined by HPLC or GC-FID analysis. Reaction conditions: ketone/aldehyde (5 mM), amine (1 to 50 eq.), *Asp*RedAm (1 mg mL^{-1}), $NADP^+$(1 mM), GDH (0.2 mg mL^{-1}), D-glucose (30 mM), Tris buffer (100 mM, pH 9.0), 25°C, 250 rpm, 24 h. [a] Only the product of double reductive amination was observed.

Table 2. Comparison of stereochemical outcomes from biotransformations catalysed by *Asp*RedAm variants W210A and Q240A.

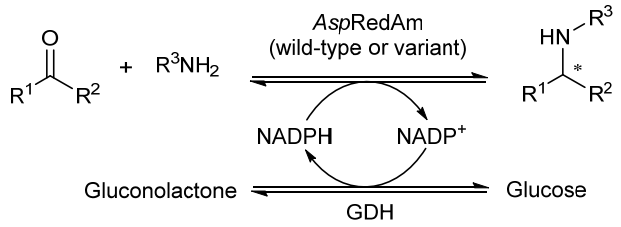

Entry	*Ketone*	*Amine*	*Product*		Asp*RedAm WT*		Asp*RedAm Q240A*		Asp*RedAm W210A*	
					Conv. (%)	***e.e.* (%) (*R* or *S*)**	**Conv. (%)**	***e.e.* (%) (*R* or *S*)**	**Conv. (%)**	***e.e* (%) (*R* or *S*)**
1	**17**	**c**	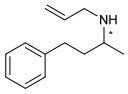	**17c**	>97	30 (*R*)	90	90 (*R*)	>97	94 (*S*)
2	**17**	**d**	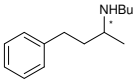	**17d**	>97	96 (*R*)	97	>98 (*R*)	>97	70 (S)
3	**17**	**g**	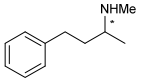	**17g**	72	85 (*R*)	>97	>97 (*R*)	>97	90 (*S*)
4	**17**	**k**	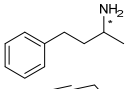	**17k**	0	n.a.	56	>98 (*R*)	0	n.a.
5	**29**	**a**		**29a**	64	95(*R*)	>97	>98 (*R*)	65	31 (*S*)
6	**9**	**a**	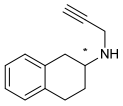	**9a**	>97	88 (*R*)	>97	>97 (*R*)	>97	80 (*S*)
7	**10**	**c**	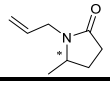	**10c**	>97	59[a]	>97	85[a]	>97	49 [a][b]

[a] Absolute configuration not assigned [b] gives opposite enantiomer to the wild-type enzyme. n.a. not applicable. N.B. Reactions carried out with 20 amine eq except for entry 5 (50 eq.). *Asp*RedAm variant Q240A displayed improved (*R*)-selectivity compared to the wild-type enzyme whereas W210A mutant was (*S*)-selective for investigated substrates.

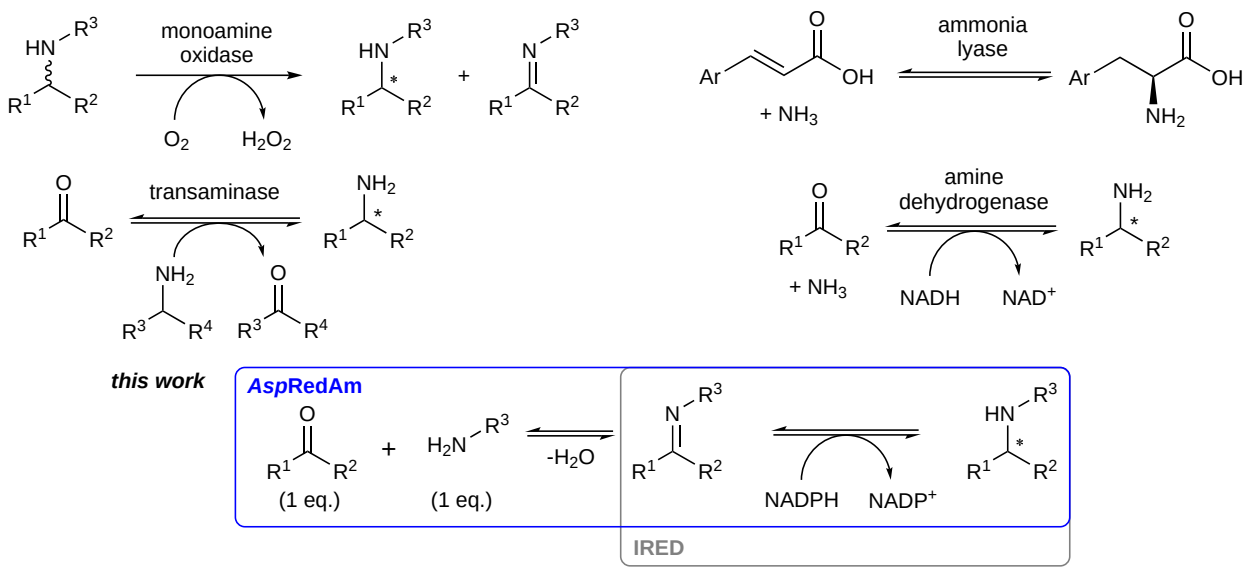
monoamine oxidase
O2
H2O2
ammonia lyase
+ NH3
transaminase
amine dehydrogenase
NADH
NAD+
this work
AspRedAm
(1 eq.)
(1 eq.)
-H2O
NADPH
NADP+
IRED

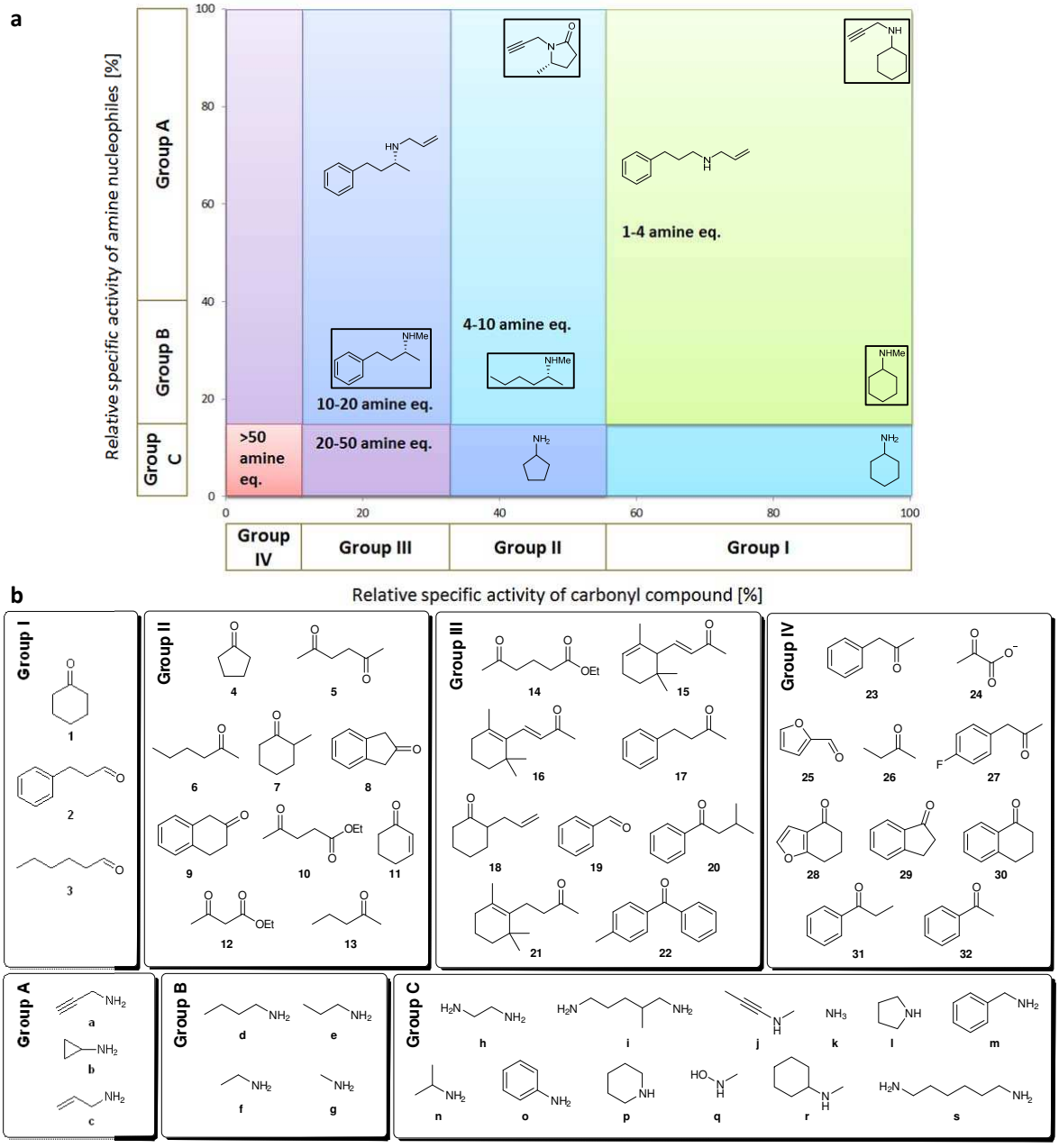

c

Reactivity Area	Specific activity range (U/mg)	Recommended ratio of amine in reductive amination
	2-9	1-4
	1-2	4-10
	0.4-1	10-20
	0.1-0.4	20-50
	<0.1	amination unlikely

Figure 2. Reactivity chart for *Asp*RedAm-catalysed reactions based on specific activities of a panel of carbonyl compounds and amine reacting partners. a) Chart displaying relative activity of amine/carbonyl pairs in reductive amination reactions. Compounds presented in the plot area are representative examples of products obtained in biotransformations. Conversions of >50% were achieved in all cases when the recommended amine:ketone ratios were used. Framed structures correspond to scaled-up biotransformations with isolated products. b) Carbonyl acceptors and amine nucleophiles arranged in Groups based on their average relative specific activity value. c) Legend for the reactivity chart with specific activity ranking and recommended ratio of amine to carbonyl compound for reductive amination.

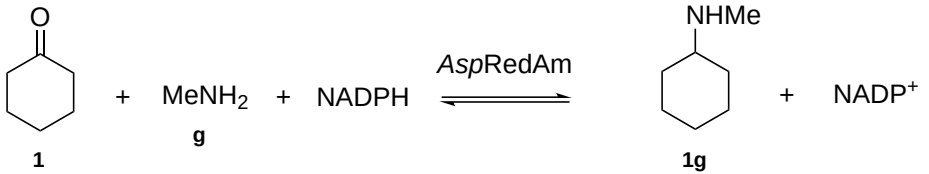
O
1
+
MeNH2
g
+
NADPH
AspRedAm
NHMe
1g
+
NADP+

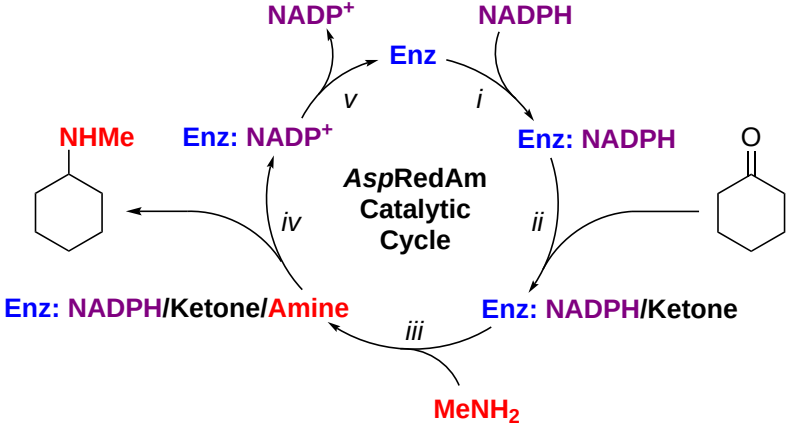
NADP+
NADPH
Enz
v
i
NHMe
Enz: NADP+
Enz: NADPH
O
AspRedAm
Catalytic
Cycle
iv
ii
Enz: NADPH/Ketone/Amine
Enz: NADPH/Ketone
iii
MeNH2

a

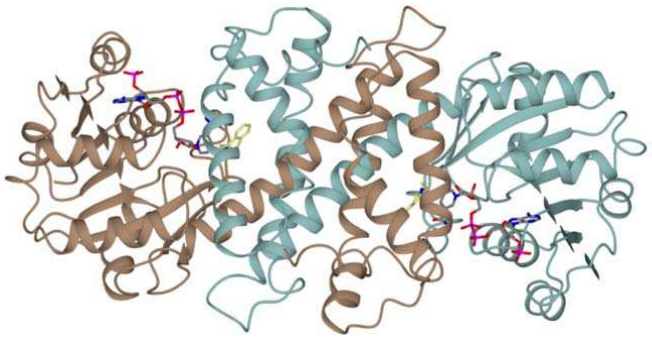

b

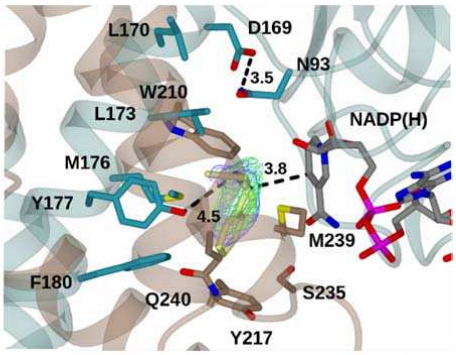

c

Enzyme variants	K_m (mM)	k_{cat} (s^{-1})	k_{cat}/K_m (s^{-1} mM^{-1})	K_m (ketone)	k_{cat} (s^{-1})	k_{cat}/K_m (s^{-1} mM^{-1})
wild-type	0.352	3.243	9.213	1.901	1.470	0.733
D169A	1.101	0.016	0.014	2.700	0.008	0.003
D169N	0.320	0.009	0.028	2.080	0.007	0.003
Y177A	0.689	0.063	0.091	2.212	0.050	0.023

Figure 4. Structural and mutagenesis data of *Asp*RedAm highlighting essential catalytic residues. a) Dimeric structure of *Asp*RedAm in complex with NADP(H) and (*R*)-29a dimer in which the active site is at the interface between the Rossman fold of one monomer and the C-terminal bundle of its neighbour; b) Active site of *Asp*RedAm at dimer interface. Electron density represents the $2F_o$-F_c (blue) and F_o-F_c (omit, green) maps, the latter obtained prior to refinement of the ligand, and contoured at levels of 1.0 and 2.5σ respectively. Distances are shown in Ångstroms. c) Kinetic data of *Asp*RedAm wild-type and mutants D169A, D169N and Y177A. Mutation at D169 and Y177 resulted in a marked decrease in activity suggesting essential roles for these residues in catalysis.

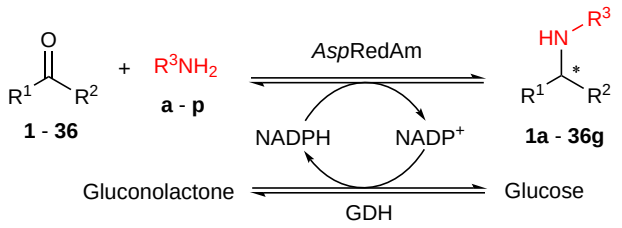

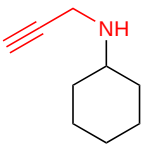

1a, (1 eq.), 94% conv.

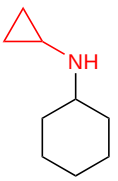

1b, (1 eq.), 90% conv.

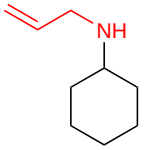

1c, (1 eq.), 73% conv.

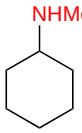

1g, (2 eq.), 95% conv.

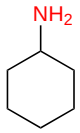

1k, (4 eq.), 47% conv.

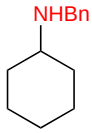

1m, (1 eq.), 84% conv.

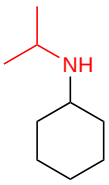

1n, (20 eq.), 94% conv.

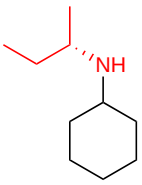

(*S*)-**1t**, (20 eq.), 81% conv.

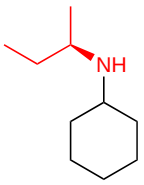

(*R*)-**1t**, (20 eq.), 10% conv.

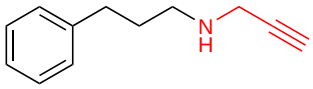

2a, (4 eq.), 97% conv.

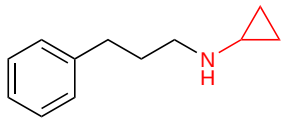

2b, (4 eq.), >97% conv.

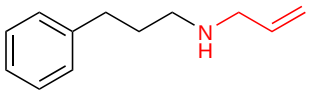

2c, (4 eq.), >97% conv.

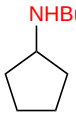

5d, (20 eq.), 93% conv.

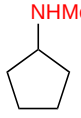

5g, (4 eq.), 81% conv.

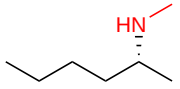

6g, (2 eq.), 72% conv.
>98% *e.e.* (*R*)

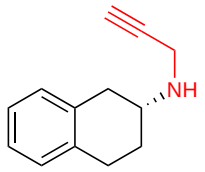

9a, (5 eq.), 45% conv.
97% *e.e.* (*R*)

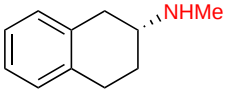

9g, (5 eq.), 39% conv.
88% *e.e.* (*R*)

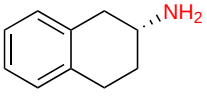

9k, (20 eq.), 37% conv.
97% *e.e.* (*R*)

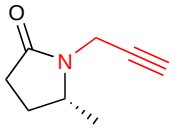

10a, (20 eq.), >97% conv.
97% *e.e.* (*R*)

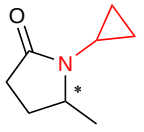

10b, (20 eq.), >97% conv.
82% *e.e.*

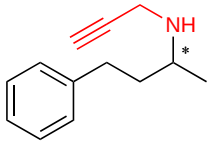

17a, (20 eq.), >97% conv.

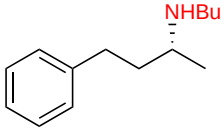

17d, (50 eq.), >97% conv.
96% *e.e.* (*R*)

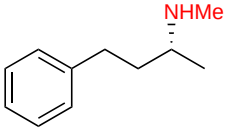

17g, (50 eq.), >97% conv.
85% *e.e.* (*R*)

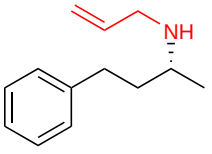

17c, (50 eq.), >97% conv.
30% *e.e.* (*R*)

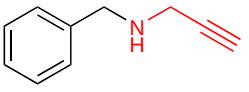

19a, (4 eq.), 92% conv.

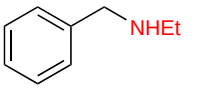

19f, (4 eq.), >97% conv.

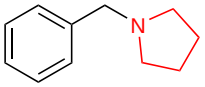

19l, (2 eq.), 58% conv.

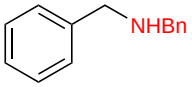

19m, (4 eq.), >97% conv.

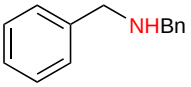

19m, (4 eq.), 50% conv.[a]

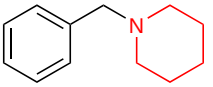

19p, (20 eq.), 40% conv.

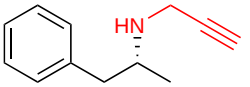

23a, (50 eq.), >97% conv.
>98% *e.e.* (*R*)

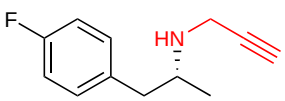

27a, (5 eq.), 49% conv.
97% *e.e.* (*R*)

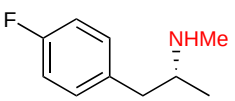

27g, (20 eq.), 54% conv.
>98% *e.e.* (*R*)

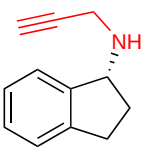

29a, (50 eq.), 64% conv.
95% *e.e.* (*R*)

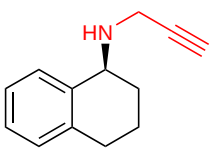

30a, (50 eq.), 15% conv.
>98% *e.e.* (*S*)

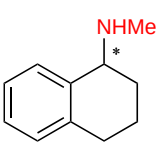

30g, (50 eq.), <5% conv.

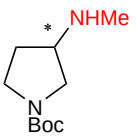

35g, (10 eq.), 53% conv.

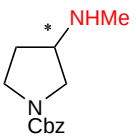

36g, (10 eq.), 64% conv.

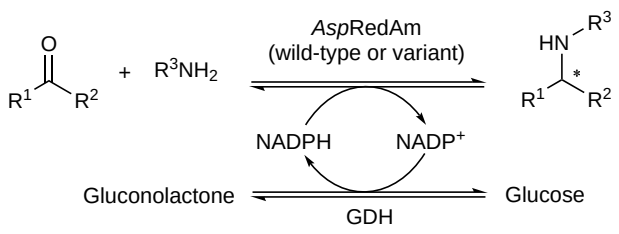
AspRedAm
(wild-type or variant)
NADPH
NADP+
Gluconolactone
Glucose
GDH

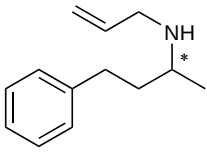
NH

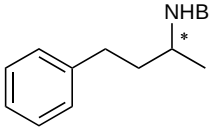
NHBu

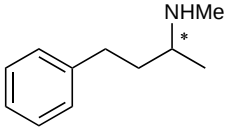
NHMe

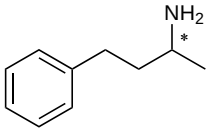
NH2

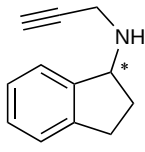
NH

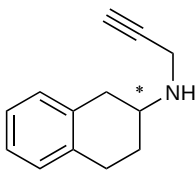
NH

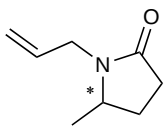
O
N